SUPPLEMENTAL INFORMATION

The supplemental information includes 11 figures, 2 tables, and supplemental methods.

SUPPLEMENTAL TABLES

Table S1. Differentially expressed genes in TIME cells co-cultured with CAFs compared with those co-cultured with NFs

See the Excel file attachment.

Table S2. Secretory ligands that are overexpressed in CAFs compared with in normal fibroblasts and that have been shown to activate c-Fos/c-Jun signaling pathways

Gene symbol	Gene name	Subcellular localization	Type
CYR61	Cysteine-rich angiogenic inducer 61	Extracellular space	Other
HGF	Hepatocyte growth factor	Extracellular space	Growth factor
IGF1	Insulin-like growth factor 1	Extracellular space	Growth factor
MFAP5	Microfibrillar associated protein 5	Extracellular space	Other
MIF	Macrophage migration inhibitory factor	Extracellular space	Cytokine
OSM	Oncostatin M	Extracellular space	Cytokine
TGFB1	Transforming growth factor beta 1	Extracellular space	Growth factor
THBS1	Thrombospondin 1	Extracellular space	Other

SUPPLEMENTAL FIGURE LEGENDS

Figure S1. Endothelial LPP Expression in HGSC Is Correlated with Amount of Fibrosis.

Micrographs of Picro Sirius Red staining for collagen on HGSC tissue samples expressing high or low levels of endothelial LPP showed that HGSC patients with high levels of endothelial LPP expression had significantly higher collagen coverage and density than did patients with low levels of endothelial LPP expression**,** suggesting an increase in fibrosis in tumor tissue with higher endothelial LPP expression (mean ± SD; N=12 per group; Mann-Whitney *U* test).

Figure S2. Silencing of LPP in Endothelial Cells Does Not Affect Cell Proliferation.

Bar chart showing that hMEC-1 endothelial cell proliferation was not significantly affected by the transfection of *LPP*-targeting siRNAs (mean ± SEM of three independent experiments; two-tailed Student *t*-test).

Figure S3. Identification of AP1 Transcription Factor–Binding Sites in the LPP Promoter Sequence.

Multiple AP1-binding sites within 1500 bp upstream of the LPP transcription start site were identified using the Biobase ExPlain analysis platform (Biobase Biological Databases). Analysis of the LPP promoter sequence suggested that increased c-Fos/c-Jun expression transcriptionally upregulates *LPP* expression.

Figure S4. Fibroblast-Derived MFAP5 Enhances Intratumoral Microvessel Formation.

(A) Luciferase-labeled imaging of A224 ovarian cancer cells showed that mice that had been subcutaneously co-injected with ovarian cancer cells and MFAP5-overexpressing ovarian fibroblasts developed larger tumors than did mice co-injected with cancer cells and control ovarian fibroblasts or cancer cells alone.

(B) A box plot showing that the weights of tumors arising from A224 cells co-cultured with

MFAP5-overexpressing fibroblasts were significantly higher than were those arising from A224 cells cultured with control fibroblasts (P=0.003). The boxes in the box plot represent the interquartile range of the records, and the lines across the boxes indicate the median tumor weight. The whiskers indicate the highest and lowest values among the records that are no greater than 1.5 times the interquartile range (N=5 per group; Mann-Whitney *U* test).

(C) Micrographs of Immunolocalization of MFAP5 and CD34 indicated that mice co-injected with A224 cancer cells and MFAP5-overexpressing fibroblasts had higher densities of CD34-positive microvessels in ovarian tumors than did mice injected with A224 cancer cells and control fibroblasts. The arrows indicate microvessels.

(D) Dot plots showing that mice co-injected with A224 cancer cells and MFAP5-overexpressing fibroblasts had higher stromal MFAP5 expression and the CD34-positive microvessels density than did the control mice (P<0.01) (mean ± SD; Mann-Whitney *U* test).

(E) Micrographs showing that endothelial *Lpp* expression in tumors that formed from tumor cells co-injected with MFAP5-transfected fibroblasts was significantly higher than that in tumors formed from tumor cells co-injected with control fibroblasts, suggesting that fibroblast-derived MFAP5 upregulated endothelial *LPP* expression. Bar=50 μm.

Figure S5. Abrogation of MFAP5-Enhanced Tube Formation by Endothelial Cells via LPP Silencing.

(A and B) Micrographs and bar charts showing that exogenous MFAP5 protein induced marked increases in total tube length, total tube area, number of segments, and number of branch points in hMEC-1 cells (A) and TIME cells (B). This induction was abrogated in cells transfected with *LPP*-targeting siRNAs but not cells transfected with control scrambled siRNA. Green: endothelial cells; bar=100 μm; (mean ± SEM of three independent; two-tailed Student *t*-test).

Figure S6. Exogenous MFAP5 Does Not Affect in Endothelial Cell Proliferation.

Bar chart showing that recMFAP5 protein treatment did not significantly affected hMEC-1 endothelial cell proliferation (mean ± SEM of three independent experiments; two-tailed Student *t*-test).

Figure S7. LPP Mediates the Effect of MFAP5 on Focal Adhesions and Stress Fiber Formation.

(A) Fluorescent micrographs showing that that hMEC-1 MECs transfected with *LPP*-targeting siRNAs had fewer F-actin stress fibers and focal adhesions than did cells transfected with control scrambled siRNA, suggesting that *LPP* plays important roles in stress fiber and focal adhesion formation. Vinculin/LPP staining was used to determine the number of focal adhesions. Red: F-actin/vinculin; green: LPP; blue: nuclei; bar=5 μm (mean ± SD; N=10 for each treatment group; two-tailed Student *t*-test).

(B) Fluorescent micrographs showing that *MFAP5*-induced formation of stress fibers and focal adhesions was abrogated in hMEC-1 cells transfected with *LPP*-targeting siRNAs and treated with recMFAP5 but not in cells transfected with scrambled siRNA and treated with recMFAP5, suggesting that *LPP* mediates the effect of MFAP5 in increasing stress fiber formation and focal adhesions. Red: F-actin/vinculin; green: LPP; blue: nuclei; bar=5 μm (mean ± SD; N=10 for each treatment group; two-tailed Student *t*-test).

Figure S8. CAF-Derived MFAP5 Increases Paclitaxel Uptake and Suppresses Tumor Growth *In Vivo*.

(A) *In vivo* study showed that mice injected with a mixture of OVCA432 ovarian cancer cells and MFAP5-overexpressing fibroblasts had significantly larger tumor burdens than did mice injected with a mixture of OVCA432 ovarian cancer cells and control fibroblasts after 2 weeks of weekly

paclitaxel (3.5 mg/kg) administration via the tail vein, suggesting that *MFAP5* confers paclitaxel resistance to OVCA432 ovarian cancer cells (mean ± SD; N=10 per group; Mann-Whitney *U* test).

(B) Fluorescent micrographs showing that ovarian tumor tissues from mice injected with *MFAP5*-overexpressing fibroblasts had a significantly higher FITC-dextran signal than did mice injected with control fibroblasts**,** suggesting that *MFAP5* increases vessel leakiness in the tumor tissue of these mice. Green: FITC-dextran; bar=100 μm.

(C) Fluorescent micrographs showing that the fluorescent-labeled paclitaxel signal in ovarian tumor tissues harvested from mice injected with *MFAP5*-overexpressing fibroblasts was significantly lower than that in tumor tissues from control mice, suggesting that *MFAP5* reduces the delivery of paclitaxel via blood vessels to cancer cells and subsequently decreases the agent's bioavailability to cancer cells in these mice. Green: Oregon Green 488-paclitaxel; bar=100 μm.

Figure S9. Western Blot Analysis of Key Signaling Pathways Mediated by MFAP5 in TIME Cells.

(A) *MFAP5*-induced FAK phosphorylation was inhibited in TIME cells loaded with the calcium chelator BAPTA/AM.

(B) Pretreatment with an anti-$\alpha_V\beta_3$ integrin antibody but not an anti-α_5 antibody or control IgG abrogated MFAP5-induced FAK phosphorylation in endothelial cells, suggesting that such induction is mediated via the engagement of $\alpha_V\beta_3$ integrin receptors.

(C) MFAP5 induced PLC-γ1 phosphorylation in endothelial cells, but this induction was attenuated in cells pretreated with an anti-$\alpha_V\beta_3$ integrin antibody, suggesting that MFAP5-induced PLC-γ1 phosphorylation is mediated via $\alpha_V\beta_3$ integrin receptors. (Western blot analysis of FAK [Figure S9B] and PLC-γ1 [Figure S9C] was performed on the same protein gel and

therefore shares the same GAPDH blot.)

(D) p-PKCθ expression was higher in the absence of the FAK inhibitor PF573228 in MFAP5-treated endothelial cells, suggesting that *MFAP5*-induced PKCθ phosphorylation is FAK dependent.

(E) p-PLC-γ1 expression was higher only in the absence of the FAK inhibitor PF573228 in *MFAP5*-treated endothelial cells, suggesting that *MFAP5*-induced PLC-γ1 phosphorylation is also FAK dependent.

(F) The *MFAP5*-induced upregulation of p-PKCθ expression was abolished in endothelial cells treated with the PLC inhibitor U71322 but not in those treated with a control solvent (DMSO).

(G) Pretreatment with a PKC inhibitor abolished the *MFAP5*-induced upregulation of p-PLC-γ1 expression in TIME cells. (Note: The blot grouping for phosphorylated PLC-γ1 was generated from multiple gels that were run in parallel.)

(H–K) The calcium chelator BAPTA/AM inhibited the *MFAP5*-induced phosphorylation of PKCθ (H), PLC-γ1 (I) (Note: The blot grouping for phosphorylated PLC-γ1 was generated from multiple gels that were run in parallel.), ERK1/2 (J) (Note: The blot grouping for ERK1/2 was generated from multiple gels that were run in parallel.), and CREB (K) in TIME cells, suggesting that these *MFAP5*-mediated signal transductions are calcium dependent.

(L–N) The *MFAP5*-induced phosphorylation of ERK1/2 was abolished in TIME cells pretreated with a PKC inhibitor. Subsequently, pretreatment of TIME cells with an ERK1/2 inhibitor abolished the *MFAP5*-induced phosphorylation of MLC2, which is essential for the formation of focal adhesion complexes (M), and the *MFAP5*-induced phosphorylation of CREB (N) (Note: The blot grouping for phosphorylated CREB was generated from multiple gels that were run in parallel).

(O and P) Pretreatment with a CPB/CREB interaction inhibitor attenuated the MFAP5-induced phosphorylation of c-Jun (O), whereas pretreatment with the c-Jun inhibitor SP600125

abrogated the *MFAP5*-induced upregulation of *LPP* expression (P) in TIME cells.

(Q) Silencing of *LPP* by transfection with *LPP*-targeting siRNAs abolished *MFAP5*-induced FAK phosphorylation at Y861 in TIME cells. The relative normalized protein expression levels with respect to the corresponding controls (indicated by the same colors, with controls having a baseline expression level of 1) are shown.

Figure S10. Western Blot Analysis of Key Signaling Pathways Mediated by MFAP5 in hMEC-1 Microvascular Endothelial Cells.

(A) *MFAP5*-induced FAK phosphorylation was inhibited in hMEC-1 cells loaded with the calcium chelator BAPTA/AM.

(B) Pretreatment with an anti-$\alpha_V\beta_3$ integrin antibody, but not an anti-α_5 antibody or control IgG, abrogated *MFAP5*-induced FAK phosphorylation in hMEC1 cells, suggesting that this induction is mediated via the engagement of $\alpha_V\beta_3$ integrin receptors.

(C) Pretreatment with an anti-$\alpha_V\beta_3$ integrin antibody attenuated *MFAP5*-induced PLC-γ1 phosphorylation in endothelial cells, suggesting that MFAP5-induced PLC-γ1 phosphorylation is mediated by $\alpha_V\beta_3$ integrin receptors.

(D) p-PKCθ expression in *MFAP5*-treated endothelial cells was increased only in the absence of the FAK inhibitor PF573228, suggesting that *MFAP5*-induced PKCθ phosphorylation is FAK dependent.

(E) Similarly, p-PLC-γ1 expression in MFAP5-treated endothelial cells was increased only in the absence of the FAK inhibitor PF573228, suggesting that *MFAP5*-induced PLC-γ1 phosphorylation is also FAK dependent.

(F) The *MFAP5*-induced upregulation of p-PKCθ expression was abolished in endothelial cells treated with the PLC inhibitor U71322 but not in those treated with a control solvent (DMSO).

(G) Pretreatment with a PKC inhibitor abolished the *MFAP5*-induced upregulation of p-PLC-γ1

expression in hMEC-1 cells.

(H–K) Treatment with the calcium chelator BAPTA/AM inhibited the *MFAP5*-induced phosphorylation of PKCθ (H), PLC-γ1 (I), ERK1/2 (J), and CREB (K), suggesting that these *MFAP5*-mediated signal transductions are calcium dependent.

(L–N) Pretreatment with a PKC inhibitor abolished the phosphorylation of ERK1/2 in *MFAP5*-treated hMEC-1 cells (L). Subsequently, pretreatment with an ERK1/2 inhibitor abolished the *MFAP5*-induced phosphorylation of MLC2, which is essential for the formation of focal adhesion complexes (M), and the *MFAP5*-induced phosphorylation of CREB (N).

(O and P) In hMEC-1 cells, pretreatment with a CPB/CREB interaction inhibitor attenuated the MFAP5-induced phosphorylation of c-Jun (O), whereas pretreatment with the c-Jun inhibitor SP600125 abrogated the *MFAP5*-induced upregulation of LPP expression (P).

(Q) Silencing of *LPP* by *LPP*-targeting siRNA transfection abolished MFAP5-induced FAK phosphorylation at Y861 in hMEC-1 cells. The relative normalized protein expression levels with respect to the corresponding controls (indicated by the same colors, with controls having a baseline expression level of 1) are shown.

Figure S11. Proposed Signaling Pathways by which MFAP5 Induces LPP Expression and Increases the Permeability and Motility of Endothelial Cells via Cytoskeleton Rearrangement.

An illustration showing that the activation of the *MFAP5*-mediated signaling cascade in endothelial cells upregulates LPP expression and subsequently promotes the motility of endothelial cells and the permeability of the endothelial cell monolayer.

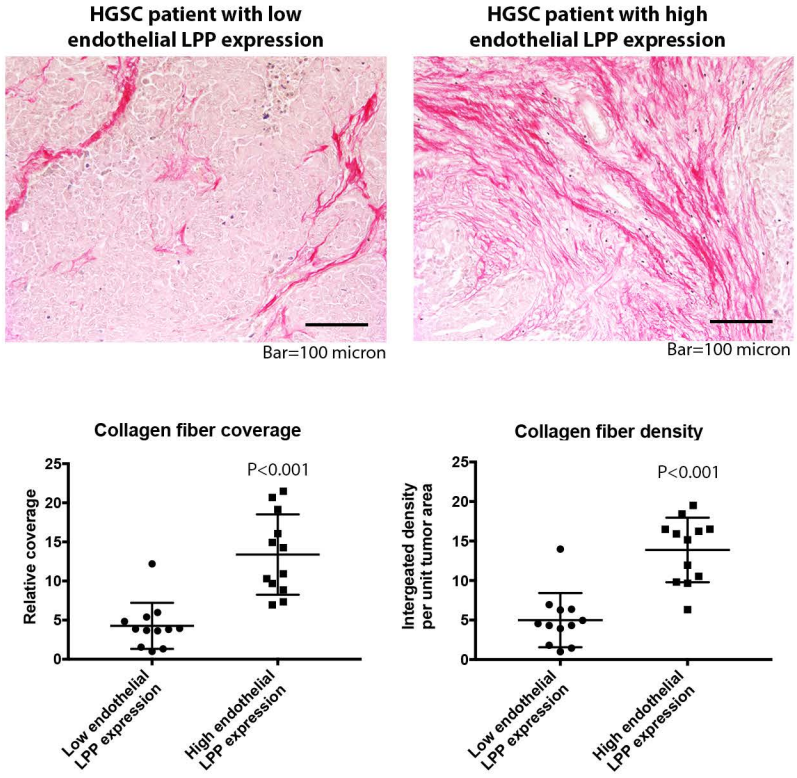

Supplemental figure S1

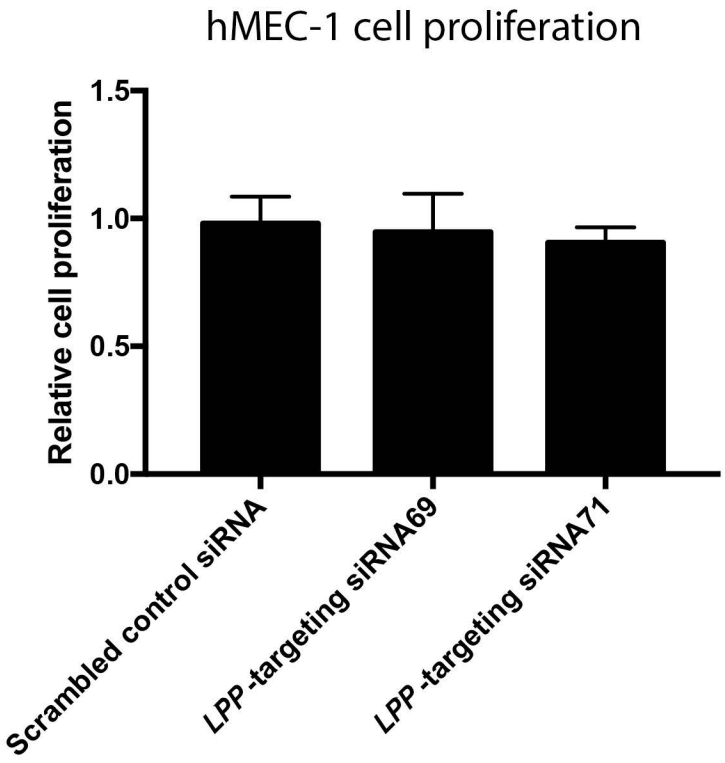

Supplemental figure S2

LPP promoter

```
-1500    AACAGAACCA CCGGGAAGCC AAGATGTGGT ACTTGGATTC CCATCTCGGA GCACCTCCTA   -1441
-1440    TATCCCGACA CACCATTTCC CCTAGTGTCT GATCTCTCTT TCTCCTCCTT TAATTCAGTC   -1381

                                                                AP1-binding site 1
-1380    TGGAGTCATT TTAGATCAGA TTCATTCCTG ATTGGCTTCA CTGCTCCAAC TTAGTCATCA   -1321
-1320    CAGAACCTTA GGGTTGGAAT CCATGTTACA AGTTAAACTG AGCAATTCAC CCCCACTTTT   -1261

         AP1-binding site 2
-1260    CCTGACAACA GTGTTCTCTT GAGAGTCTGG TTTTATTCTG AGTCTTCCAG CCCGGTGTCT   -1201
-1200    GTGCCCATGA AGGACTCATG CCAAATTACA TTCTCAGGAG GACTCCCAGA CCAAGAGACT   -1141
-1140    CTGGGCTTGG GCGTGAGAGA CTTGGGGCTG TTCTTTTTCT TTTTTTTTTT TTGAGAAGAA   -1081

                                    AP1-binding site 3
-1080    GTTTCACTCT TATTGCCCAG GCTGACATGG AGTTTCACTC TTATTGCCCA GGCTGGAGTG   -1021

                         AP1-binding site 4
-1020    CAATGGCACA GTCATGGCTC ACTGCAACCT CCGCCTCCCG GGTTCAAGTG ATACTCCTGC   -961
 -960    CTCAGCCTCC CAAGTAGCTG GGATTACAGG CACACACCAC CATGCCTGGC TAATTTTTGT   -901

                                                                AP1-binding site 5
 -900    ATTTTTAGTA GAGACCAGTT TTCACCATGT TGGCCAGGCT GGTCTTGAAC TCCTGACCTC   -841

                                                    AP1-binding site 6
 -840    AGGTGATCCT CCCGCCTTGG TCTCCCAAAG TGCTGGGATT ACAGGTGTGA GCCACTGTGC   -781
 -780    CCGGCCGAGA GGAGTTGTTT TGAGACTCAC CTGCCATCAT AGGAACCATA GCTTAAATTC   -721
 -720    TTGTGACCTT TTCAGGTGCA TCTCCCAAAA TATCTCCCCT CCACCAAATT AATGATTTAT   -661
 -660    TTCATAAATT TAGTTGCATT CTGGATGGTC TCATTCTTAA GATGAGCTTA AAGCCTTTCA   -601
 -600    GACCAGTCAC TTCCTTGTTT GGGGTGGAGG AGGTTTTTTC CTGGAATAGG ACAGTGTATG   -541
 -540    GAAGGGTTGA GAATCCACTT CTTTAGCGGT TAATAATTTA CTCCGAGTAA GGAATTCTTT   -481
 -480    GTTAAAGTGG GGCATGTTCT TCAAGTGCCA GAGAAGAGAG AAGGGTGATT TTTCTGACAT   -421

                                          AP1-binding site 7
 -420    CCTCCAGCCT GCTTCTCCAT ATTTGGAAAT GTTTACCCAC CAGGCTGATC TATTGGAAGA   -361
 -360    GAGGGAGGTG ACTCAGGGTT TAGGAGAAGC AGGATTTGAA TTCTTGTTTC CAGAAACAAA   -301
 -300    GTCGTCCCCC CACCCTGCCC CCACCCTTCC CCCTTCATTC CTCTGTCCCT TGTTCTGGAA   -241
 -240    GCTGAGGCGA GAATGTCTCA GTTCTGTTCC CTTCAGGCTT CGAGACCACC GCCTTGCTGT   -181
 -180    GTCCCGTAGT GGACTGAGGG CCTGCAAGAG GGAGTGAGGG CTAGTGGAGG GCCAGCTGCC   -121
 -120    TGTGGGGGCT GGACATCGTG TGAGTACATC ATTACTGCCA TTTCTGCTCA CAGACCTGGG   -61

                                AP1-binding site 8
  -60    GCTTACAGCC TGTGGGCTGG CTCACTTGCA TGGTGATGGG ACACGTTGCT GGGAGTGCTG   -1

Transcription start site
    1    GTCACTTTTA TTTGGGGGTG TGGACAGCTG CTTTCCCAGG GGAGTACTTC TTACAGTGGG    60
         ..........................................................................................

                Start codon
  241    CCAACAATGT CTCACCCATC TTGGCTGCCA CCCAAAAGCA CTGGTGAGCC CCTCGGCCAT    300
```


Supplemental figure S3

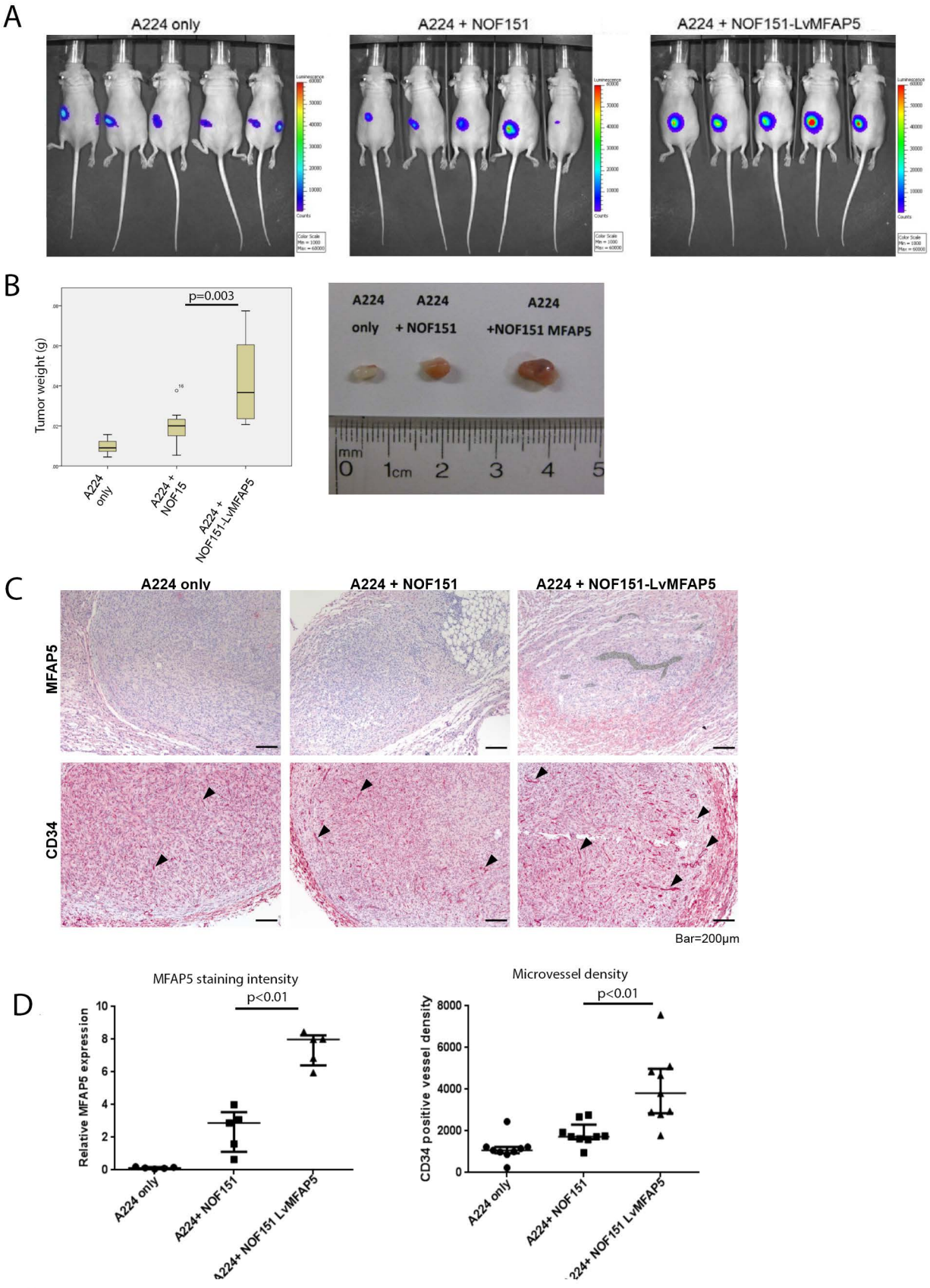

Supplemental figure S4

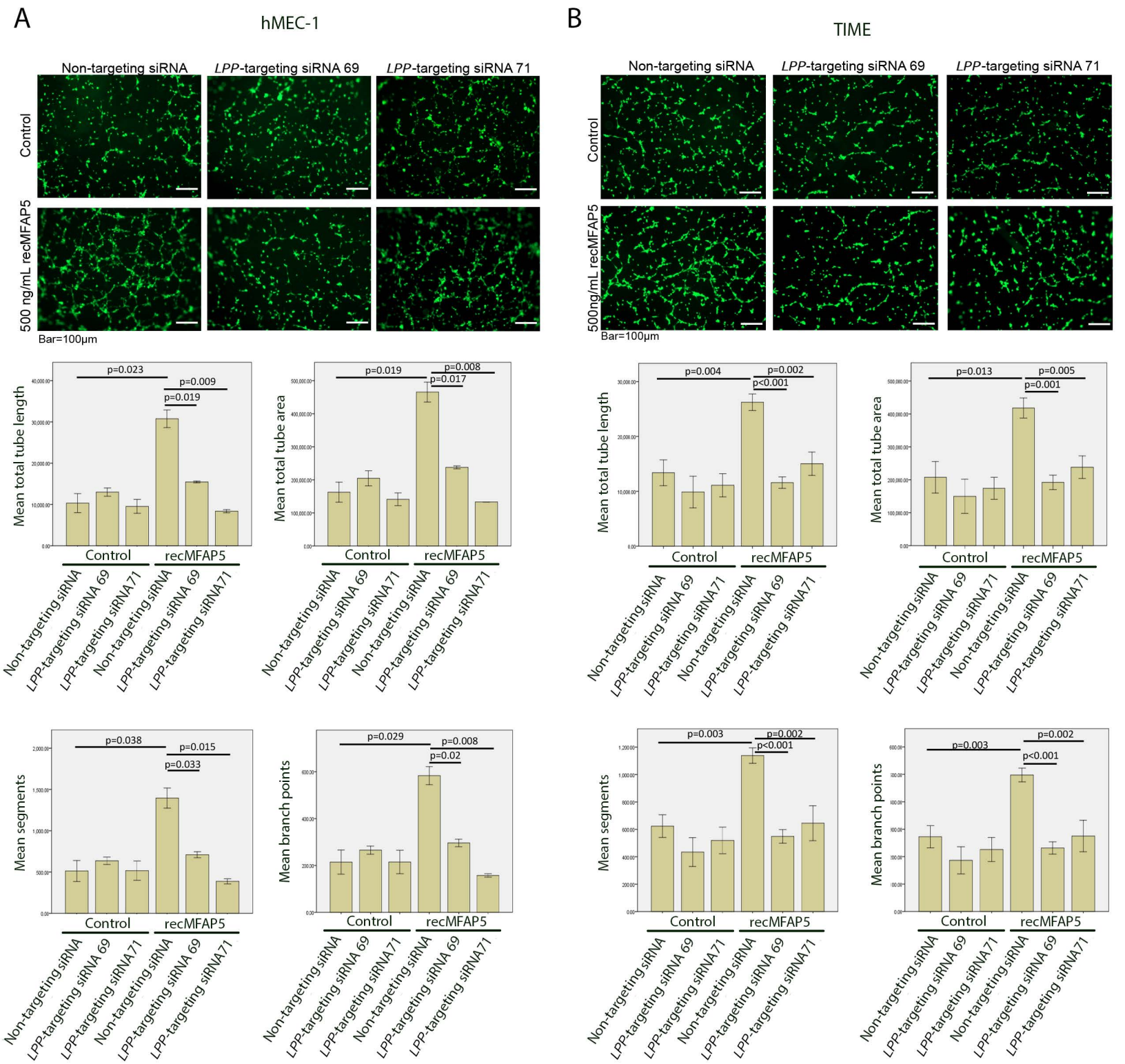

Supplemental figure S5

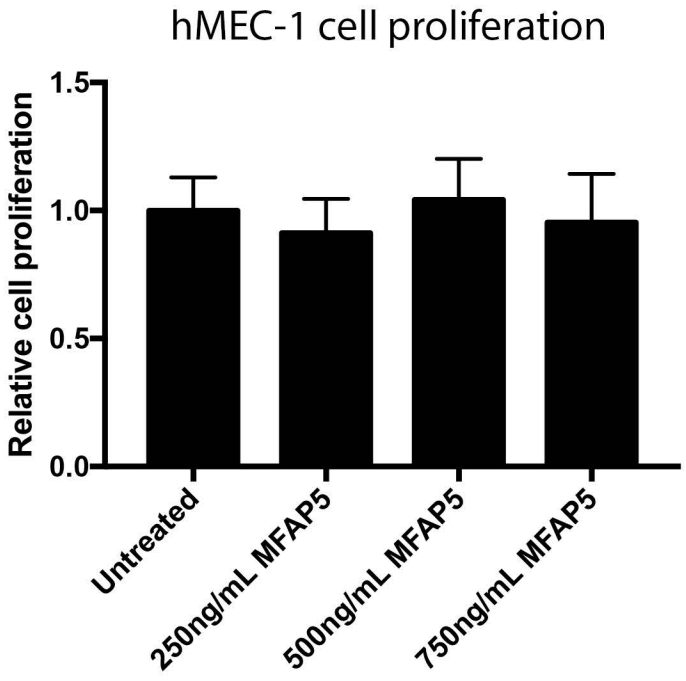

Supplemental figure S6

A

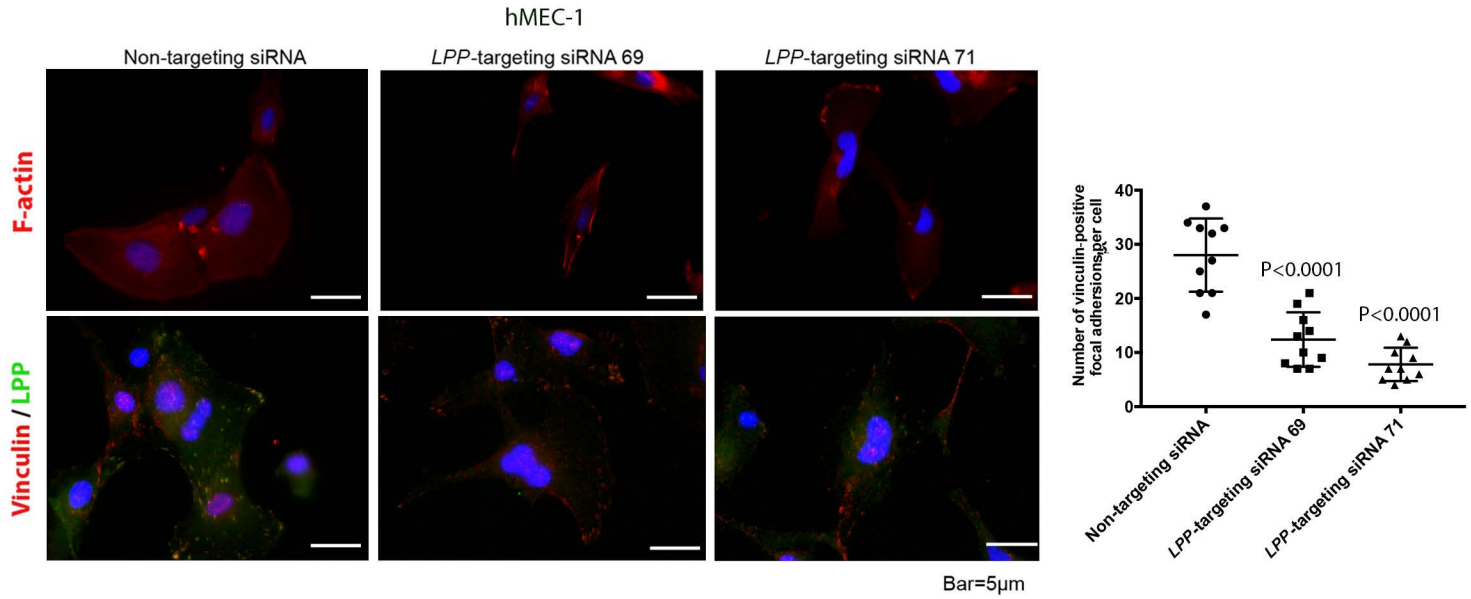

B

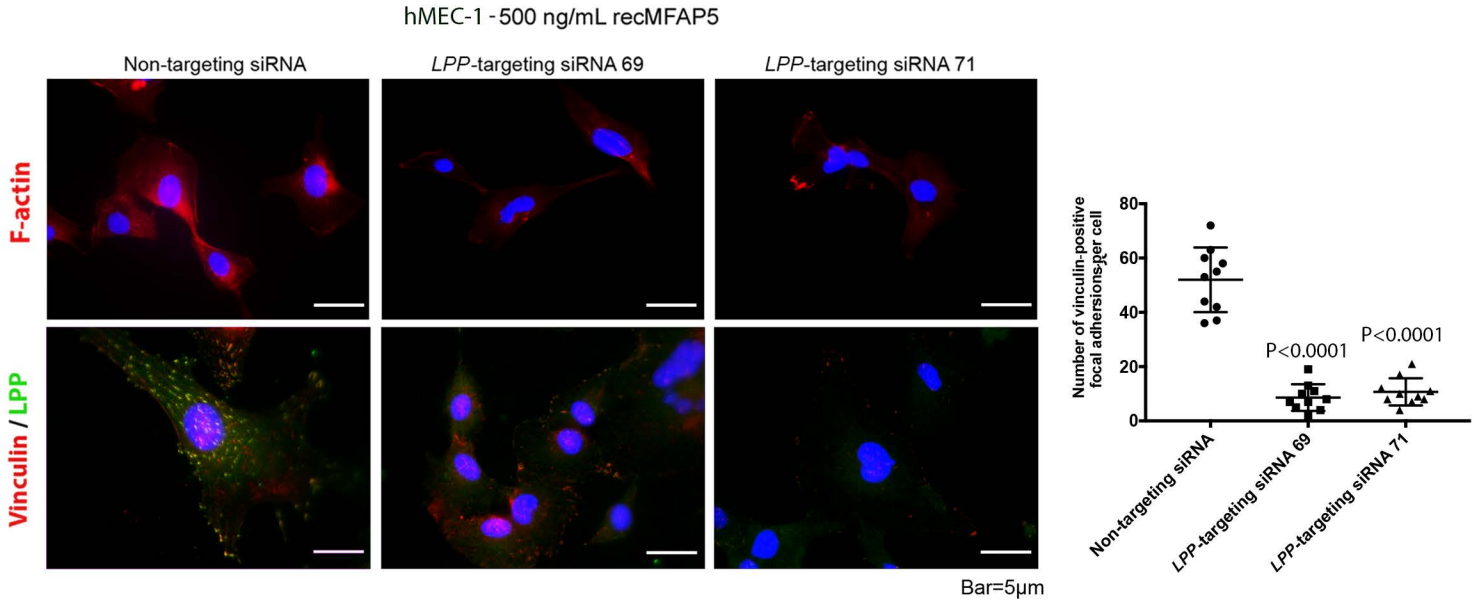

Supplemental figure S7

A

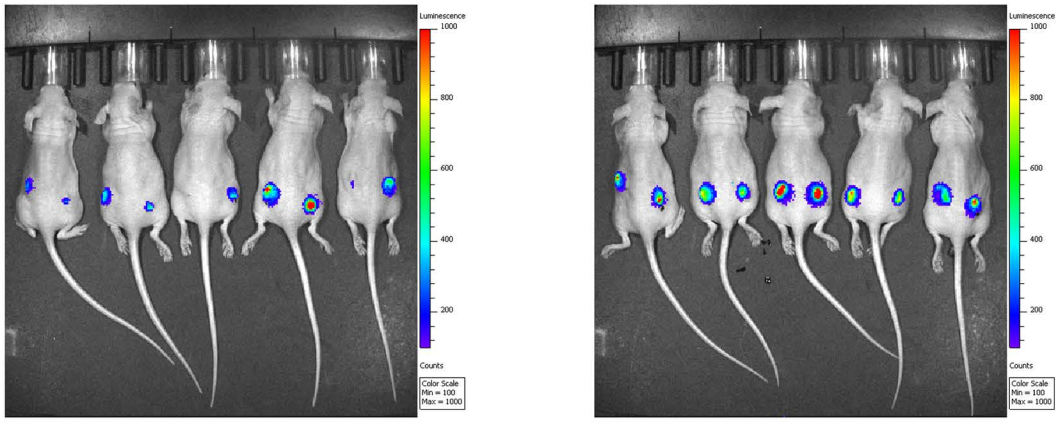

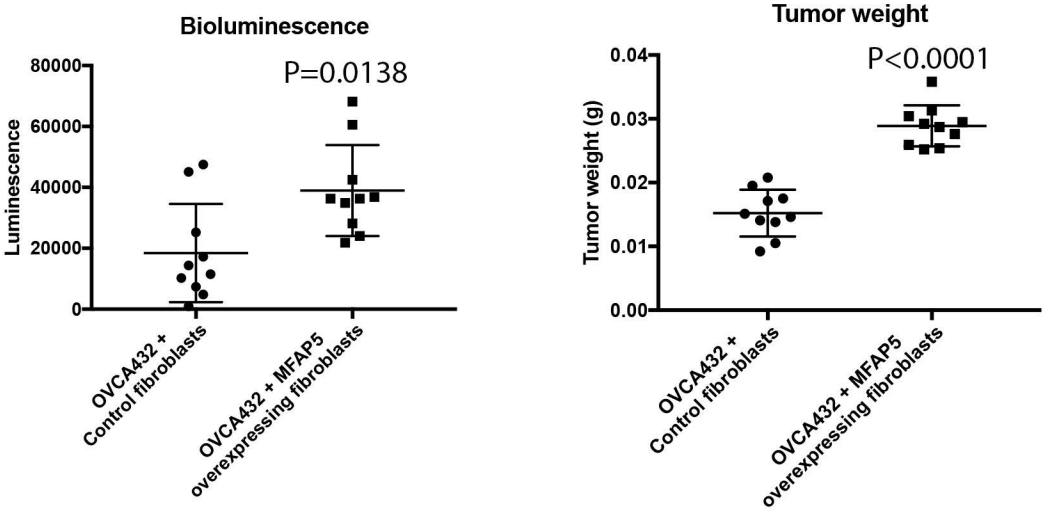

B

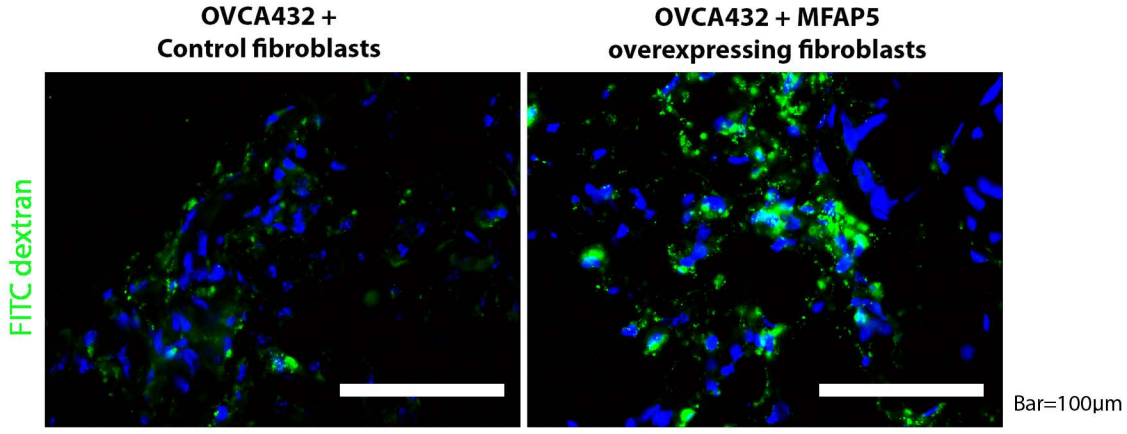

C

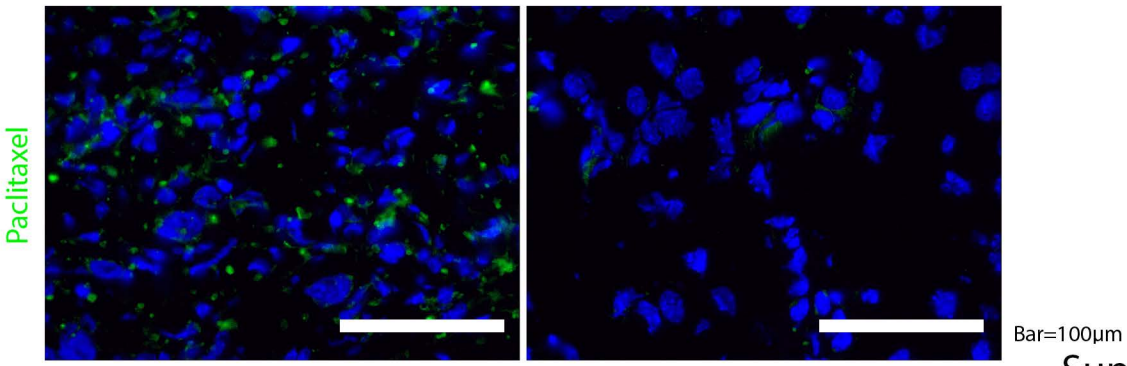

Supplemental figure S8

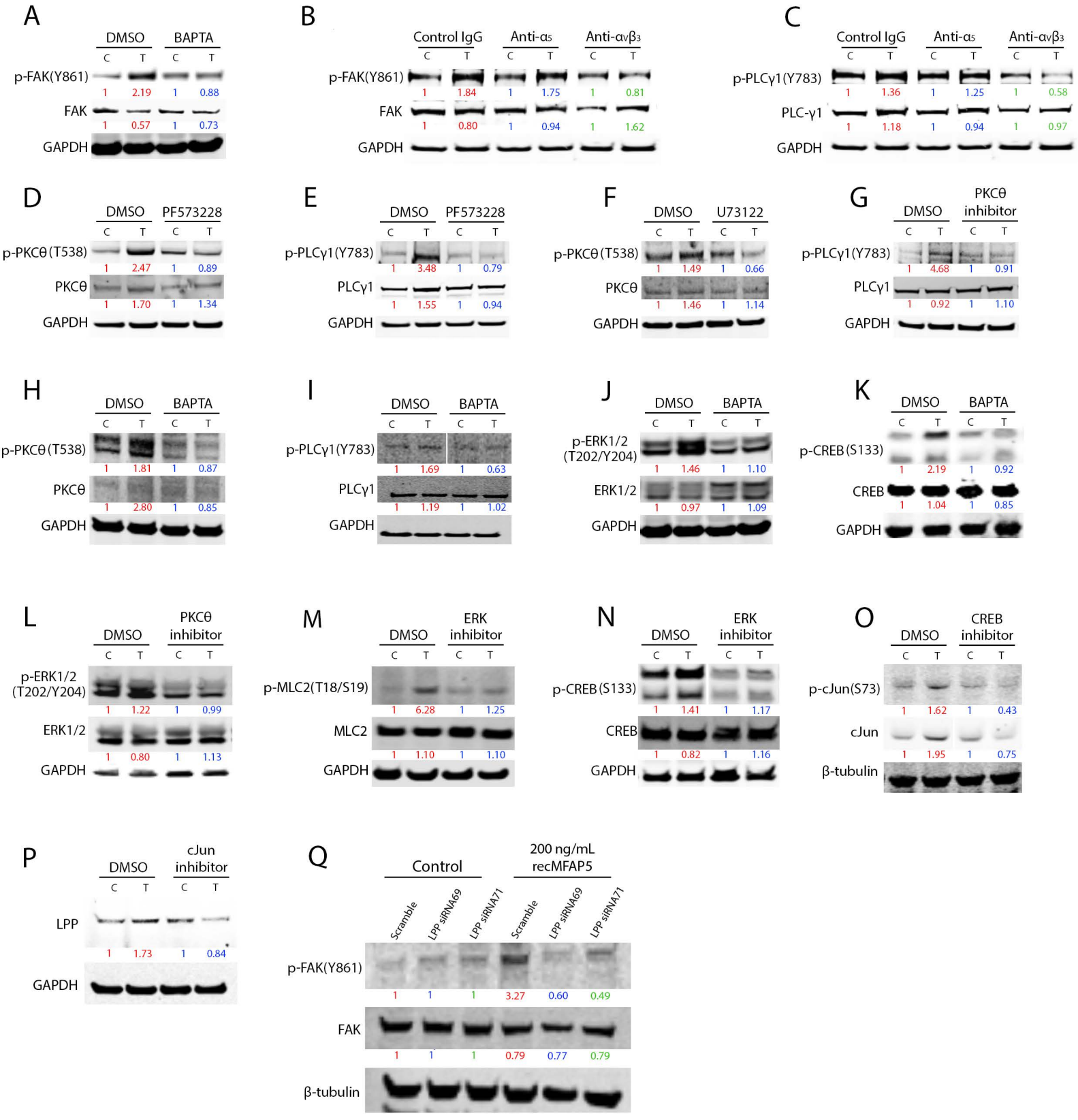

Supplemental figure S9

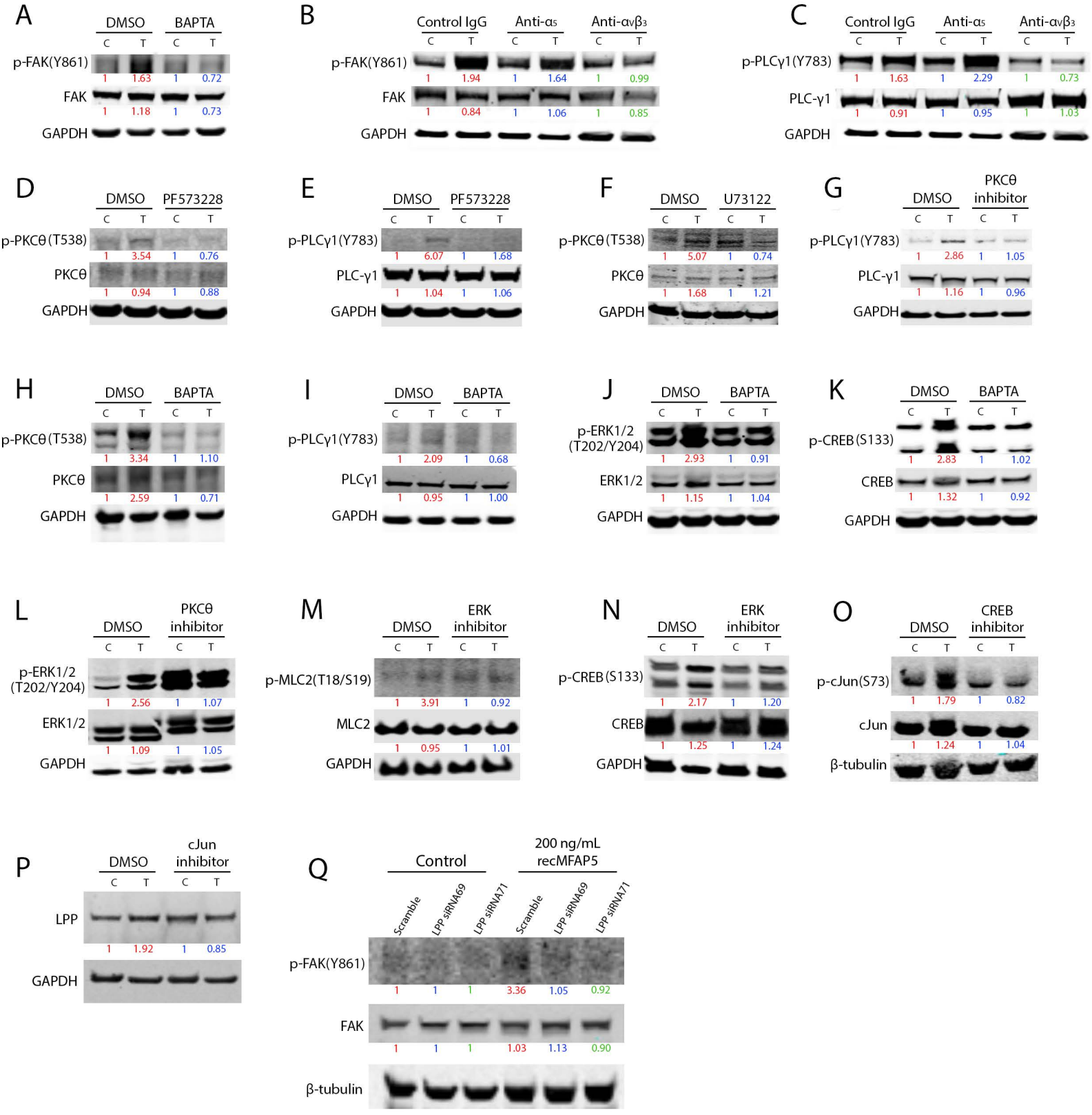

Supplemental figure S10

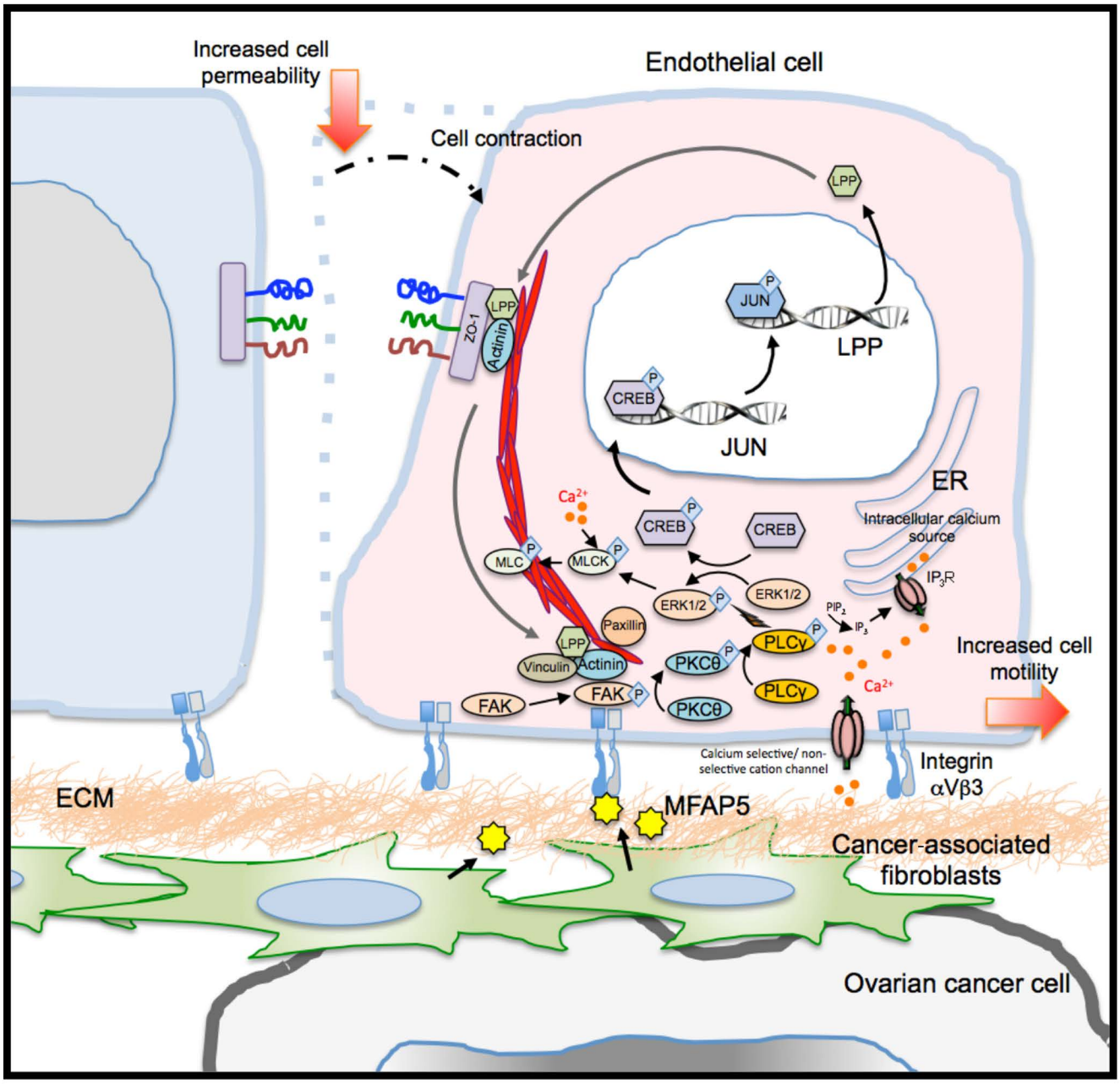

Supplemental figure S11

SUPPLEMENTAL METHODS

Transcriptome Profiling of Microvascular Endothelial Cells. To investigate the effects of CAFs on tumor angiogenesis, we co-cultured 1 x 10^4 TIME human MECs with either 2 x 10^4 primary ovarian CAFs or 2 x 10^4 normal ovarian fibroblasts (NFs) in Boyden chambers. Endothelial cells were harvested 48 hours after cell seeding and total RNA was isolated and purified. A transcriptome analysis of the RNA samples was performed using the GeneChip Clariom D assays (Affymetrix) according to the manufacturer's protocol. Differentially expressed genes (expression fold change > 1.5; moderated t-test and Benjamini-Hochberg multiple testing adjusted p-value <0.05) were identified using the Genespring GX Bioinformatics Suite (Version 14.9; Agilent Technologies). The list of upregulated genes in endothelial cells induced by CAFs was analyzed using the Ingenuity Pathway Analysis software program to identify associated biological functions.

Quantitative Real-Time Polymerase Chain Reaction Analysis. The relative expression of each target gene was calculated using the $2^{-\Delta\Delta CT}$ method to calculate the average CT value of the housekeeping gene for a single reference gene value. Predesigned human MFAP5 (Hs00185803_m1), LPP (Hs00944352_m1), cyclophilin A (Hs99999904_m1), and murine Mfap5 (Mm00489404_m1) TaqMan gene expression assays (Life Technologies) were used in quantitative real-time polymerase chain reaction analyses.

Western Blot Analysis. Protein lysates from microvascular endothelial cells were separated on 10% sodium dodecyl sulfate NuPAGE gels under denaturing conditions and transferred onto nitrocellulose membranes using an iBlot Western blotting system (Life Technologies) before being incubated with primary antibodies. Anti-human MFAP5 (#HPA010553) was purchased from Sigma-Aldrich. An anti-phosphorylated-FAK antibody (Y861; #44-626G) was purchased

from Life Technologies. All other antibodies, including anti-FAK (#3285), anti-PLC-γ1 (#2822), anti-phosphorylated-PLC-γ1 (T783; #2821), anti-PKCθ (#2059), anti-phosphorylated-PKCθ (T538; #9377), anti-ERK1/2 (#9102), anti-phosphorylated ERK1/2 (T202/204; #9101), anti-CREB (#9197), anti-phosphorylated CREB (S133; #9198), anti-c-Jun (#9165), anti-phosphorylated c-Jun (S73; #9164), anti-MLC2 (#8505), anti-phosphorylated MLC2 (T18/S19; #3674), and anti-LPP (#3389) antibodies, were purchased from Cell Signaling Technology. After being washed with Tris-buffered saline with Tween, the membranes were incubated with a goat anti-rabbit infrared dye-conjugated secondary antibody (LI-COR Biosciences). Protein bands were detected using an Odyssey infrared imaging system (LI-COR Biosciences). Protein expression levels, normalized according to the corresponding GAPDH or beta-tubulin controls, were calculated on the basis of the band intensity values measured using the ImageJ software program (National Institutes of Health).

The inhibitors used in pathway analyses included a PLC inhibitor (U73122; #sc-3574), PKCθ pseudo substrate inhibitor (#sc-3097), and ERK inhibitor II (FR180204; #sc-203945), which were purchased from Santa Cruz Biotechnology. FAK inhibitors (SU6656, #S9692; PF-573228, and #PZ0117) and a c-Jun inhibitor (#SP600125) were purchased from Sigma-Aldrich, and a CBP/CREB interaction inhibitor (#217505) was purchased from EMD Millipore.

CAF Co-Culture Promoted Endothelial Cell Motility via *LPP* Expression. To evaluate the roles of CAFs on tumor angiogenesis, a motility assay was performed using Boyden chambers in a 24-well plate: 8 x 10^4 TIME cells were seeded onto each 8-μm porous cell culture insert (BD Biosciences). In the lower chamber, no cells, 1.6 x 10^5 NFs, or 1.6 x 10^5 CAFs were plated. After a 4-hour incubation period, endothelial cells were stained with calcein AM (Life Technologies). Non-migrated endothelial cells in the cell culture inserts were removed, and the

endothelial cells that migrated through the pores were quantified by obtaining images of the stained cells in nine random fields of view per membrane using fluorescent microscopy and the Image-Pro Plus software program (version 7.0). The experiment was repeated with TIME cells transfected with either scrambled siRNA or one of the two efficiency-evaluated *LPP*-targeting siRNAs (Silencer Select #s8271, #s8269; Life Technologies) to determine whether the effects of CAFs on endothelial motility are mediated through endothelial *LPP* expression.

CAF Co-Culture Promoted Endothelial Cell Monolayer Permeability via *LPP* Expression. An i*n vitro* monolayer permeability assay was performed to evaluate the effects of CAFs on the permeability of the TIME cell monolayer. FITC-dextran (20 mg/mL; relative molecular mass, 70,000 Da; Sigma-Aldrich) was added to the confluent TIME cell monolayers seeded onto 0.4-μm porous cell culture inserts in the absence of NFs or CAFs in the lower chamber. The appearance of fluorescence in the bottom wells of the Boyden chambers was monitored by analyzing 40-μl medium aliquots in a time course using a FLUOstar Omega microplate reader (BMG Labtech). The passage of FITC-dextran through the endothelial cell monolayer culture was used to assess the permeability and integrity of the monolayer culture. The experiment was repeated with TIME cells transfected with either scrambled siRNA or one of the two *LPP*-targeting siRNAs to determine whether the effects of CAFs on endothelial monolayer permeability are mediated through endothelial *LPP* expression.

***LPP* Mediates the Effect of MFAP5 on Endothelial Cell Motility.** To evaluate the roles of MFAP5-induced *LPP* expression in angiogenesis, we performed a motility assay using Boyden chambers with hMEC-1 and TIME cells. Serum-free MCDB131 and EBM-2 medium, with or without 50 ng/mL recMFAP5, was incubated with 10 μg/mL control IgG or anti-MFAP5, anti-αVβ3, or anti-α5 antibodies for 1 h in the wells of 24-well plates. Next, 8 x 10^4 hMEC-1 or TIME

cells were seeded onto each 3- or 8-μm porous cell culture insert, respectively (BD Biosciences), with serum-free medium and placed in the 24-well plate containing the preincubated cell culture medium. After a 4-h incubation period, endothelial cells were stained with calcein AM (Life Technologies). Non-migrated ovarian cancer cells in the cell culture inserts were removed, and the endothelial cells that migrated through the pores were quantified by obtaining images of the stained cells in nine random fields of view per membrane using fluorescent microscopy and the Image-Pro Plus software program (version 7.0).

To determine the roles of calcium and *LPP* in cell motility induced by MFAP5, we pretreated microvascular endothelial cells with the cell-permeant calcium chelator BAPTA/AM (B-6769; Life Technologies) at a concentration of 10 μM for 1 h or transfected the cells with *LPP*-targeting siRNA before performing the motility assay.

Effect of MFAP5 on Endothelial Cell Monolayer Permeability. hMEC-1 or TIME cells (1 x 10^4) were seeded onto each well of an E-plate of the xCELLigence system (Roche Applied Bioscience) and incubated at 37°C for 24 h to obtain a confluent monolayer endothelial cell culture. The next day, cell culture media in the wells were replenished with serum-free MCDB131 or EBM-2 medium, with or without 200 ng/mL recMFAP5. Electrical impedance generated by the monolayer endothelial cells on gold electrodes was measured throughout the course of the experiment using a real-time cell analyzer as the cell index. Decreased cell adhesion or monolayer integrity was indicated by a drop in the cell index value.

An *in vitro* monolayer permeability assay was also performed to verify that MFAP5 enhanced the permeability of the endothelial cell monolayer using the xCELLigence system. FITC-dextran (20 mg/mL; relative molecular mass, 70,000 Da; Sigma-Aldrich) was added to the confluent

hMEC-1 or TIME monolayers seeded onto 0.4-μm porous cell culture inserts in the presence or absence of 200 ng/mL recombinant MFAP5. The appearance of fluorescence in the bottom wells of the Boyden chambers was monitored by analyzing 40-μl medium aliquots in a time course using a FLUOstar Omega microplate reader (BMG Labtech). The passage of FITC-dextran through the endothelial cell monolayer culture was used to assess the permeability and integrity of the monolayer culture.

Tube Formation Assay. One hundred microliters of growth factor-reduced BD Matrigel (BD Biosciences) supplemented with 200 ng/mL recMFAP5, 500 ng/mL recMFAP5, or PBS was coated onto each well of a prechilled 24-well plate. The plate was then incubated at 37°C for 1 h to allow the Matrigel to solidify. Afterward, 5 x 10^4 hMEC-1 or TIME cells were resuspended in 1 ml of serum-free MCDB131 or EBM-2 medium and seeded onto each well of the 24-well plate coated with growth factor-reduced BD Matrigel. The assay plate was then incubated at 37°C for 4 h before the cells were stained with calcein AM. Endothelial tube formation was examined using a fluorescent microscope, and the extent of tube formation among different experimental groups was quantified and compared using the angiogenesis module of the MetaMorph imaging analysis software program.

Fibroblast-Derived MFAP5 Enhances Intratumoral Microvessel Formation. We subcutaneously injected 2 x 10^6 luciferase-labeled A224 ovarian cancer cells, with or without 2 x 10^6 of NOF151-LvMFAP5 or mock-transduced NOF151 cells, into nude mice. Five days after cell injection, tumor progression was monitored and quantified via luciferase-based imaging using an IVIS 200 bioluminescence and fluorescence imaging system. On day 12, all mice were euthanized and weighed. Tumors were collected, fixed in formalin, and processed for histological evaluation.

LPP Mediated MFAP5 Stimulation of Calcium-Dependent F-Actin Rearrangement. hMEC-1 or TIME cells (5 x 10^4) were seeded onto eight-well Lab-Tek chamber slides (Thermo Fisher Scientific) and serum-fasted for 24 h. After serum starvation, cells were treated with fresh serum-free medium, supplemented with or without 200 ng/mL recMFAP5. After 4 h of incubation, cells were fixed with 3.7% formaldehyde and stained with Alexa Fluor 594 phalloidin (Life Technologies), according to the manufacturer's instructions, to visualize the F-actin cytoskeleton. Fluorescent microscopy was used to evaluate the MFAP5-induced F-actin cytoskeleton rearrangement in cells.

To determine the role of calcium in MFAP5-induced F-actin cytoskeleton rearrangement, we pretreated microvascular endothelial cells with the cell-permeant calcium chelator BAPTA/AM (B-6769; Life Technologies) for 1 h before treatment with MFAP5 and staining with Alexa Fluor 594 phalloidin. To determine the effect of LPP on F-actin reorganization induced by MFAP5, microvascular endothelial cells were transfected with *LPP*-specific siRNA before treatment with MFAP5 and staining with Alexa Fluor 594 phalloidin.

$[Ca^{2+}]i$ Measurement. hMEC-1 cells that grew on collagen-coated Petri dishes with glass bottoms were loaded with Fluo-4 AM in Hank's balanced salt solution for 30 min, followed by 20 min to de-esterify the dye. Fluo-4 AM was excited at 488 nm, and its emission was measured using a bandpass filter at 522/35 nm. Fluorescent images of the cells were collected using a TCS SP5 confocal microscope at 0.25 Hz.

Immunofluorescent Labeling of LPP and Focal Adhesion Markers. hMEC-1 or TIME cells (5 x 10^4) were seeded onto eight-well Lab-Tek chamber slides and serum-fasted for 24 h. After serum starvation, cells were treated with fresh serum-free medium, supplemented with or

without 200 ng/mL recMFAP5, for 24 h. After incubation, cells were fixed with 3.7% formaldehyde and stained with an anti-LPP antibody (1:100; Cell Signaling Technology) or an anti-vinculin antibody (1:100; Life Technologies) at ambient temperature for 2 h, followed by a 1-h incubation with the Alexa Fluor 488 goat anti-mouse IgG antibody (1:1000; Life Technologies). Slides were then mounted with ProLong Diamond Antifade Mountant (#P36961; Life Technologies), and fluorescent microscopy was performed to evaluate the expression and localization of LPP and vinculin in endothelial cells.

To determine whether MFAP5-induced LPP expression localized at the focal adhesion complexes of endothelial cells, LPP and the focal adhesion marker vinculin, paxillin, or FAK were immunolocalized in MFAP5-treated endothelial cells via sequential immunostaining with an anti-LPP antibody (1:100; Cell Signaling Technology), followed by staining with an anti-vinculin antibody (1:100, #700062; Life Technologies), anti-paxillin antibody (1:50, #AF4259; R&D Systems), or anti-FAK antibody (1:100, #3285; Life Technologies).

To determine the role of LPP in focal adhesion formation induced by MFAP5, microvascular endothelial cells were transfected with LPP-specific siRNA before treatment with MFAP5 and staining with anti-LPP and anti-vinculin antibodies.